Continental Shelf Research 30 (2010) 781–792

Contents lists available at ScienceDirect

Continental Shelf Research

journal homepage: www.elsevier.com/locate/csr

Two- and three-dimensional double-sandbar system behaviour under intense wave forcing and a meso–macro tidal range

R. Almar [a,b,*], B. Castelle [a,b], B.G. Ruessink [c], N. Sénéchal [a,b], P. Bonneton [a,b], V. Marieu [a,b]

[a] Université de Bordeaux, CNRS, UMR EPOC 5805, Av. de Facultés, Talence F33405, France
[b] CNRS, UMR EPOC 5805, Talence F33405, France
[c] Department of Physical Geography, Faculty of Geosciences, Institute for Marine and Atmospheric Research, Utrecht University, P.O. Box 80.115, 3508 TC Utrecht, The Netherlands

ARTICLE INFO

Article history:
Received 26 May 2009
Received in revised form
19 January 2010
Accepted 1 February 2010
Available online 6 February 2010

Keywords:
Double-sandbar system
Meso–macro tidal environment
Storm impact
Nearshore
Video imaging
Short-term morphodynamics
Truc Vert Beach

ABSTRACT

Five weeks of hourly, 10-min time-exposure video images were used to analyze the meso–macro-tidal double-barred Truc Vert Beach, SW France, under intense wave forcing. The four storms experienced, one of which with an offshore significant wave height over 8 m, induced dramatic changes in the double sandbar system. The subtidal outer bar migrated offshore rapidly (up to 30–50 m/day) and its pre-existing crescentic pattern was wiped out. The seaward-protruding parts of the outer bar barely migrated offshore during the most intense storm, whereas a landward-protruding part was shed off. Over the entire study period, the outer-bar dynamics was dominated by alongshore-averaged changes rather than alongshore non-uniform changes, while the opposite was observed for the inner bar. In addition, the outer-bar dynamics was predominantly controlled by the time-varying offshore wave conditions, whereas the inner-bar dynamics was influenced largely by the tide-range variations. Our observations put forward the key role of morphological settings (the presence of a subtidal bar and its shape) and tidal range in governing inner-bar behaviour within a double sandbar dynamics, and provide strong support for previous suggestions that sandbars cannot be studied in isolation.

1. Introduction

Double nearshore sandbar systems are common morphological features along sandy, wave-dominated, micro- to meso–macro-tidal coastlines (Ruessink et al., 2003; Van Enckevort et al., 2004; Castelle et al., 2007). Both bars can exhibit a wide range of planshapes, varying from linear to undulating. Alongshore non-uniformities in nearshore sandbars are traditionally classified into discrete states within the conceptual model of Wright and Short (1984). Initially developed for single-barred, micro-tidal beaches, this conceptual model identifies three main beach states from dissipative to reflective with, in-between, an intermediate state further divided into 4 sub-states. Within this intermediate state, immediately below the dissipative state is the Longshore Bar and Trough (LBT), next the Rhythmic Bar and Beach (RBB), then the Transverse Bar and Rip (TBR) and finally the Low Tide Terrace (LTT). High-energy wave conditions generally induce an up-state transition toward the LBT or the fully dissipative state, which is associated with rapid seaward bar migration of up to 10–20 m/day (e.g., Gallagher et al., 1998). During post-storm, decreasing wave-energy conditions, undulating patterns develop (down-state transition); also, the bar slowly propagates shoreward (Sallenger et al., 1985; Gallagher et al., 1998). In double bar systems, both bars are expected to go through all the states within the intermediate classification and independently follow the same up-state and down-state schemes as single-barred systems (Short and Aagaard, 1993).

Alongshore-averaged (or two-dimensional 2D) cross-shore bar migration has primarily been considered as a morphologic adjustment to the hydrodynamic forcing (among others, King and Williams, 1949; Aagaard et al., 1998). However, this theory has been recently challenged by observations (Ruessink and Terwindt, 2000; Plant et al., 2001) and numerical modelling (Aarninkhof et al., 1998; Masselink, 2004) which put forward that 2D bar behaviour is more complicated than previously envisaged. Bar dynamics may be driven by an interaction of the evolving bar itself and the hydrodynamic forcing. A bar strongly controls the wave breaking location (Lippmann and Holman, 1989) and, hence, cross-shore sediment transport patterns; this may reinforce or suppress further bathymetric modifications (e.g., Plant et al., 2001). For instance, wave-breaking across an outer bar affects the hydrodynamics and hence the evolution of an inner bar. Observations (Ruessink et al., 2007a) suggest that the distance between the inner and outer bars might be a critical parameter governing the behaviour of the composite double-bar system

* Corresponding author at: Université de Bordeaux, CNRS, UMR EPOC 5805, Av. de Facultés, Talence F33405, France. Tel.: +33 5 40 00 88 32; fax: +33 5 56 84 08 48.
E-mail address: r.almar@epoc.u-bordeaux1.fr (R. Almar).

0278-4343/$ - see front matter © 2010 Elsevier Ltd. All rights reserved.
doi:10.1016/j.csr.2010.02.001

during down-state transitions. However, the 2D, cross-shore response of double bar systems to storms is still poorly understood (e.g., Castelle et al., 2007), especially that of the inner bar.

The role of morphological feedback in forming alongshore non-uniform (three-dimensional, 3D) bar patterns is now also widely acknowledged (Coco and Murray, 2007). In double-bar systems, the outer bar often exhibits a reasonably regular crescentic pattern (Van Enckevort et al., 2004), defined as an alongshore sequence of horns and bays where horns and bays are, respectively, landward- and seaward-protruding parts. Recent observations (Ruessink et al., 2007a) and numerical modelling (Castelle et al., in press-a, in press-b) showed that the generation of 3D inner-bar patterns may be more complicated, typically being a mixture of self-organization and outer–inner-bar interactions (or "morphological coupling") rather than self-organization alone. On the contrary to the relatively well-known down-state sequence, up-state double-bar system interactions during storms, whereby pre-existing 3D patterns disappear into an alongshore 2D bar, are still poorly understood. It is possible that during up-state transitions the inner and outer bar may also strongly interact. For instance, during intense (storm) wave forcing, Wijnberg and Holman (2007) observed at a single-barred beach (Duck, USA) that a crescentic bar may shed a bar-like feature that later on merged with the subaerial beach. They named this spatially isolated feature a Shoreward Propagating Accretionary Wave (SPAW). Similar features have been described for Wanganui, New Zealand (Shand, 2007). It is possible that a SPAW shed off from an outer bar may similarly affect the evolution of an inner bar. The link between 2D and 3D changes has never been investigated for up-state transition in double-bar systems.

Recent studies have shown that the tidal range can affect bar dynamics by changing the type and duration of shoaling-wave, surf and swash processes across the bar (Masselink and Turner, 1999; Masselink et al., 2006; Price and Ruessink, 2008). A small tidal range is expected to increase surf zone and swash processes and thus to result in rather short response times to time-varying incident wave conditions, whereas a large meso- to macro-tidal range favours shoaling-wave processes and, hence, increases the response time. Curiously, despite their common occurrence (Short, 1991), double-barred systems exposed to a large tidal range have barely been studied (among others; Masselink et al., 2007, 2008). In particular, the effect of such a large tidal range on the double-bar system response to storms is poorly understood.

In this paper, we present the first high-frequency (~daily) observations of double bar dynamics in a high-energy, meso–macro-tidal environment. In Section 2, we present the hydrodynamic and video data gathered during a 5-week period of intense wave forcing at Truc Vert Beach, SW France. In Section 3, we describe the temporal evolution of this system. Also, we investigate outer–inner-bar interactions as well as the link between waves and tidal levels well seaward of the surf zone and the observed double-bar evolution. The observed complexity of the double-bar system response to storm and tide conditions is discussed in Section 4.

2. Data

2.1. Study area description

The field site is Truc Vert Beach (TVB), located along the southern part of the French Atlantic Coast (Fig. 1) and typical of the relatively undisturbed coast extending 100 km between the Gironde Estuary (90 km to the North) and the Arcachon Lagoon inlet (10 km to the south). TVB's straight sandy coastline is almost

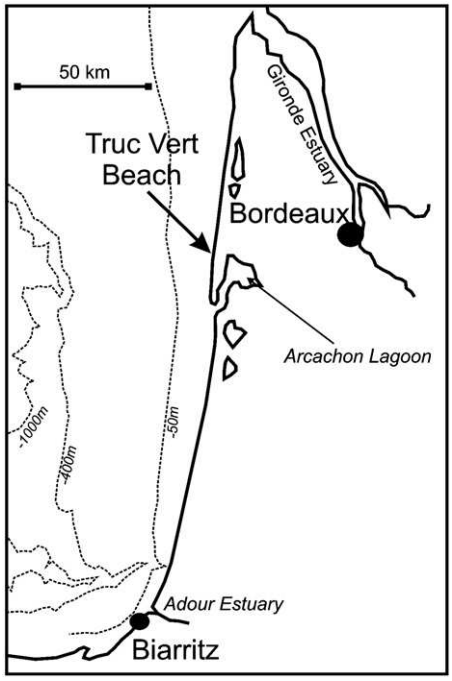

Fig. 1. Location of the field study site, Truc Vert Beach, on the French Aquitanian Coast.

N–S-oriented and bordered by high aeolian dunes. The sediment consists of quartz sand with a mean grain size ranging from 200 to 400 μm (Pedreros et al., 1996). TVB is a wave-dominated environment characterized by mainly low-steepness waves associated with long-distance swell travelling from the W-NW direction. The seasonal modulation of the incoming wave energy is strong, with a minimum in wave energy during summer; in winter the offshore significant wave height (*Hs*) may reach 10 m during severe storms. The mean annual *Hs* is 1.4 m with a corresponding mean period of 6.5 s (Butel et al., 2002). The tide is semi-diurnal with a neap and spring tidal range of about 1.5 and 5 m, respectively. TVB is a highly dynamic, intermediate double-barred beach (Castelle et al., 2007; Sénéchal et al., 2009) following the classification of Wright and Short (1984) and Short and Aagaard (1993).

Long-term satellite monitoring and monthly topographic surveys showed that the inner bar can go through all the intermediate sub-states within the classification of Wright and Short (1984). The inner intertidal bar usually exhibits a TBR morphology with a mean alongshore-averaged wavelength of about 400 m (Lafon et al., 2002; De Melo Apoluceno et al., 2002; Sénéchal et al., 2009). From recurrent observations, De Melo Apoluceno (2003) established that a significantly longer period than for other sites (Owens and Frobel, 1977) was required for the down-state transition from LBT to LTT to occur at TVB. De Melo Apoluceno (2003) suggested that waves with $Hs > 3$ m were required for enforcing an up-state from the LTT morphology, despite some observations (De Melo Apoluceno, 2003) have shown that LTT morphology can persist during storm events with $Hs > 3$ m and TBR morphology during storm events with $Hs > 5$ m. Alongshore southward migration rates of 0.5–4.5 m/day were deduced from sparse satellite images and shoreline maps, and are limited to fair weather conditions.

Most of the time the outer bar exhibits crescentic patterns with a mean alongshore wavelength of about 700 m (Froidefond et al., 1990; Castelle 2004; Lafon et al., 2004). Sparse bathymetric surveys have shown that the shallowest landward-protruding section of the bar, the deepest seaward-protruding section of the

bar and the trough are on the order of 2, 4.5 and 6 m above the Lowest Astronomical Tide (LAT), respectively (Desmazes et al., 2002). These values are likely to vary significantly given the highly-variable wave conditions TVB is exposed to, and given that the available bathymetric surveys were undertaken during fair weather conditions only. The outer-bar shape can vary from a regular crescentic shape to a strongly skewed crescentic shape (Lafon et al., 2004), presumably related to angle of wave incidence. Over a 3-month period of relatively fair weather, Lafon et al. (2004) reported a southerly migration rate of about 1 m/day.

2.2. ECORS08 wave and tide data

The ECORS (DGA-SHOM) field experiment took place at TVB from March 1 to April 9, 2008, and involved 120 scientists from 16 international institutions. One of the aims of the experiment was to study short-term TVB response to storms (more details can be found in Sénéchal et al., 2008). These storm condition expectations were fully satisfied as, during the experiment, the Aquitanian Coast was exposed to 4 severe storms with *Hs* larger than 4 m, comprising a 10-year return storm with *Hs* larger than 8 m coinciding with spring tidal ranges. Wave characteristics (*Hs*, peak period (*Tp*) and direction) were sampled half-hourly from a waverider buoy, located offshore in 54-m depth (SHOM-"Service Hydrographique et Oceanographique de la Marine"). The tidal level was obtained from prediction (SHOM). Time series of the offshore wave and tide parameters during the experiment are shown in Fig. 2.

Nearshore subtidal bathymetric surveys have been carried out by the SHOM on February 14 and April 7–9. Intertidal and subaerial beach surveys were performed daily with centimetric accuracy using DGPS (Parisot et al., 2009). Fig. 3 shows the combination of the topographic and bathymetric data on February 14, in which strikingly well-developed outer-bar crescents with a wavelength of about 600 m can be seen.

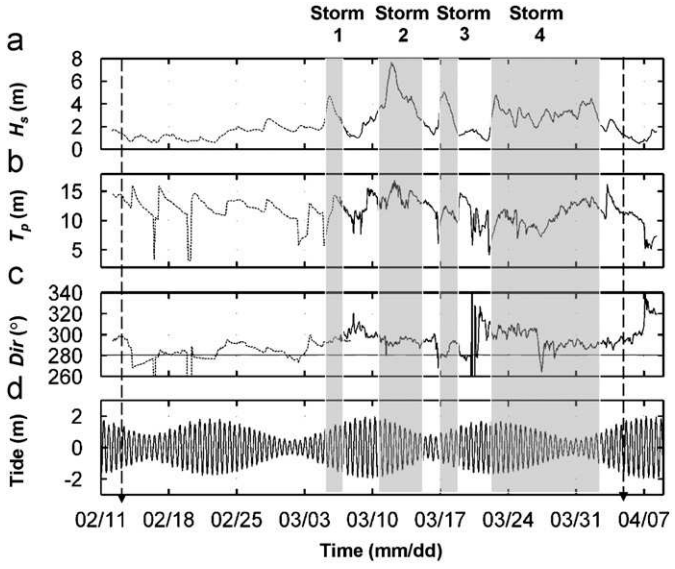

Fig. 2. Time series of offshore (a) significant wave height *Hs*, (b) peak period *Tp*, (c) angle of incidence and (d) water level (tide) versus time at Truc Vert Beach. The horizontal line in (c) indicates the shore-normal direction. Vertical grey bands correspond to the 4 storm periods described in the text. Vertical dashed arrows correspond to the initial and final bathymetric surveys.

2.3. ECORS08 video data

A video system (Cam-Era technology-NIWA) was set up for the duration of the experiment, mounted on an 8-m high scaffolding implemented on the top of the dune (27 m above the Mean Sea Level (MSL)). The system contained two high-resolution cameras (3.5 MPixel) covering an alongshore distance of the inner- and outer-bar of 1200 and 2500 m, respectively. The system collected full frames continuously at 2 Hz during daylight hours for the entire experiment. Because the storm on March 5 damaged the scaffolding, images are available from March 6 to April 9 only.

Time-exposure images were generated by averaging over 1200 consecutive images (10 min) every hour. The two camera images were rectified from pixel to world coordinates (Holland et al., 1997) and merged to yield a single plan view image, referenced to the tidal level. The grid resolution in the plan view images was $2 \times 2\,m^2$. In the inner-bar area, in front of the video cameras (x=0 m, y=0 m), the pixel footprint dimensions were about 0.5 and 1 m in the alongshore y and cross-shore x directions, respectively. These dimensions increase to about 10 and 20 m at both alongshore ends of the field site.

On the selected time-exposure images, white bands are present due to predominant wave-breaking over the underlying bar morphology (Lippmann and Holman, 1989; Van Enckevort and Ruessink, 2001). The bar-crest locations were digitalized by manually tracking the cross-shore location of the image intensity peaks in the alongshore direction. Following Van Enckevort and Ruessink (2003a, 2003b), a matrix $X(t,y)$ was constructed for both bars, consisting of bar crest locations in cross-shore direction X at time t and alongshore location y. The remotely sensed bar crest position varies in time because of time-varying offshore waves and tidal levels (Van Enckevort and Ruessink, 2001) even when the bar crest itself does not migrate. We removed this artificial migration following the approach of Pape and Ruessink (2008). On the whole, the difference between tracked and real bar-crest position depends on (1) the quality of the bar tracking, (2) the pixel footprint, (3) the photogrammetric error that mainly results from the difference between actual elevation and tidal level and (4) the tide- and wave-induced artificial shift (corrected). For the daily averaged bar crest positions, the resulting overall uncertainty in the cross-shore direction is estimated as about 20 and 10 m for the outer bar and the inner bar, respectively.

The bar-crest data were used to describe both the alongshore averaged cross-shore bar crest location $\langle X \rangle$ and the cross-shore distance D between horns and bays positions which indicates how well crescentic patterns and rip channels are developed. In addition to bar-crest lines, the alongshore position of each outer-bar horn, and the seaward exit and landward end of each inner-bar rip channel was manually digitized from the available video time-exposure images.

As we will demonstrate below, we observed a SPAW during part of the field experiment. Information on the observed SPAW morphology and evolution were derived from wave-breaking pattern on video time-exposure images. As described in Wijnberg and Holman (2007), the maximum alongshore length (L) and area of a SPAW were computed from digitized SPAW contours.

2.4. Hydro- and morphological indexes

To link offshore hydrodynamic forcing to nearshore bar morphological changes, specific indexes were computed. A new offshore hydrodynamic forcing parameter has been created, the Hydrodynamic Forcing Index (HFI) that allows representing the cumulative effect of wave and tide forcing. The HFI index is defined as the ratio of offshore significant wave height *Hs*

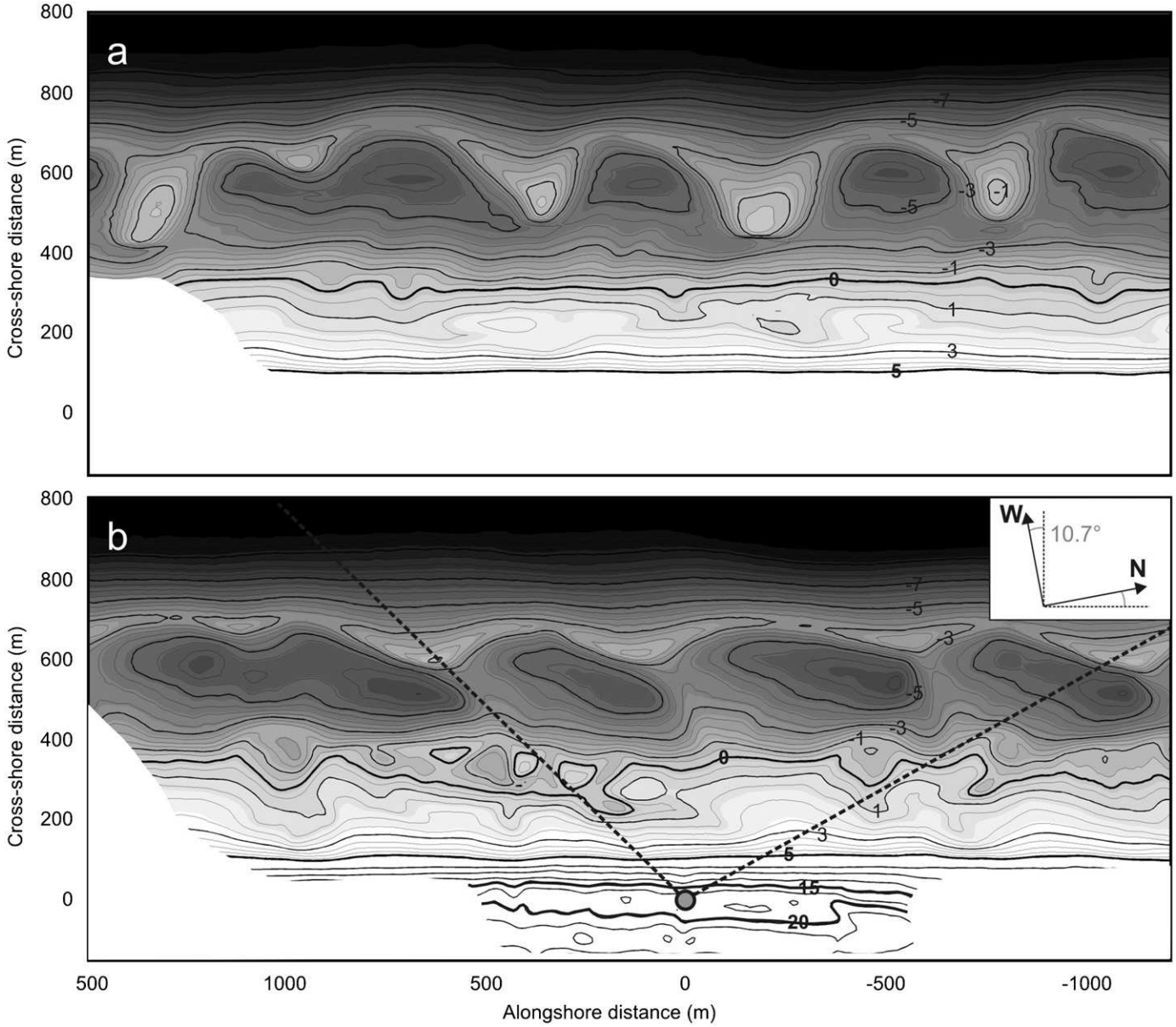

Fig. 3. Truc Vert Beach bathymetry surveyed (a) on February 14, 2008, 3 weeks before the experiment and (b) on April 6, 2008, at the end of the experiment. In (a) the circle at the origin (0,0) indicates the camera system location, and the 0- and 5-m iso-contour stand for the Lowest Astronomical Tide (LAT) and the Highest Astronomical Tide (HAT), respectively. Black dashed lines indicate the camera view field.

(averaged over a tidal cycle) to d_{min} the lowest offshore water level experienced over a tidal cycle (high–low–high tide) above the lowest astronomical tide:

$$HFI = \frac{Hs}{d_{min}} \tag{1}$$

HFI is large for large *Hs* and large tidal range, when d_{min} is low. Our choice to use a new index is motivated by the fact that the existing RTR index (ratio of *Hs* to tide range, see Masselink and Short, 1993) commonly used in inter-tidal morphodynamic studies (among others; Kroon and Masselink, 2002; Masselink et al., 2006; Price and Ruessink, 2008) is not appropriate when considering the observed enhanced impact of a storm in association with a large tide range. This would result in a rather low RTR, indistinguishable from a situation of moderate Hs and neap-tide conditions.

A simple Morphological Index (MI) was computed with the objective to represent the changes of both the inner (MI_i) and the outer-bar (MI_o). The 2D bar changes (MI_{2D}) were determined as the absolute value of the alongshore-averaged cross-shore bar migration rate:

$$MI_{2D} = \left|\frac{d\langle X\rangle}{dt}\right| \tag{2}$$

The 3D bar changes (MI_{3D}) were determined by computing the absolute variation rate of the cross-shore amplitude $A=D/2$ (mathematical definition, half the distance D between bays and horns cross-shore positions) over time,

$$MI_{3D} = \left|\frac{dA}{dt}\right| \tag{3}$$

We did not consider alongshore migration of crescentic and rip patterns in MI_{3D}. The MI index combines MI_{2D} and MI_{3D},

$$MI = \frac{MI_{2D} + MI_{3D}}{\max(MI_{2D} + MI_{3D})} \tag{4}$$

Its maximum value of 1 occurs when the combined cross-shore migration rate and amplitude change are maximum.

3. Results

3.1. Description of the evolution of the double bar system

Prior to the storm sequence, on February 14, the outer bar was characterized by well-developed and regular crescentic patterns (Fig. 3a). The alongshore-averaged wavelength was about 600 m and D_o was about 370 m, which is the largest value in our dataset and is substantially larger than observed elsewhere (e.g., Van Enckevort et al., 2004). The mean vertical difference between shallowest landward-protruding sections of the bar horns and the troughs was about 4 m. In contrast, the inner bar was reasonably alongshore uniform A 1-day storm ($Hs > 4$ m, $Tp = 14$ s) hit TVB on March 5 (Fig. 2). The tidal range during this day was intermediate, close to 3 m. Moderate wave angle with respect to shore-normal (8°, W-NW) coupled with moderate Hs induced a southerly longshore current that resulted in a southward migration of the outer-bar crescentic pattern by 20–30 m without any substantial change in the outer-bar shape (Fig. 4a). This migration was inferred by comparing the video images of March 8–February 14 survey.

The second storm that hit TVB, from March 10–13, was severe with maximum Hs of about 8 m and a corresponding Tp of 18 s, with $Hs > 4$ m during 3 days (Fig. 2). The wave angle with respect to shore-normal was about 15° (W-NW). The tidal range was close to 4 m (spring tide). Morphologic changes associated to this storm are shown in Fig. 4a and b, on March 8 and 14, respectively. The high-energy wave conditions induced an up-state transition (Wright and Short, 1984) of the outer-bar geometry that evolved from well-developed crescentic patterns to a more alongshore linear shape (D_o decreased from ~350 to ~90 m, Fig. 5a). In addition to this outer-bar straightening, the bar migrated some 100 m offshore (Fig. 5a). Interestingly, an isolated bar-like feature (that we henceforth refer to as a SPAW) shed from one of the outer-bar horns, visible as an isolated and coherent patch of foam between the inner and outer bar (Fig. 4b and c). This phenomenon and its evolution are explored in the next subsection. Due to the combined effects of large Hs and wave angle, a 150 m southward migration of the outer bar was observed (see tracked outer-bar horn positions in Fig. 6). Not following an expected up-state transition (Wright and Short, 1984), the inner-bar alongshore non-uniformity increased during the storm (D_i increased from ~30 to ~80 m, Fig. 5b), with the formation of a bulk of sand facing the transverse bar (which can be deduced from the undulating inner-bar wave-breaking pattern at about $x = 200$ m, Fig. 4c).

From March 16 to 17, TVB was exposed to a short-duration storm ($Hs = 6$ m, $Tp = 12$ s), with shore-normal waves during neap tide (tidal range of about 2.5 m). Fig. 4c and d show the plan-view images before and after this third storm, respectively. The outer bar was not substantially affected as no significant outer-bar cross-shore migration, alongshore migration and amplitude changes were observed (Fig. 5a). The SPAW that had appeared during the previous storm welded to the inner bar. As a consequence the inner-bar morphology changed significantly, with increasing alongshore non-uniformities and a slight smoothing of the inner-bar bulk of sand (Fig. 4d). The inner bar did not migrate significantly in the cross-shore direction during this storm.

After a 5-day low-energy period, the fourth storm hit TVB from March 21 to 31, which constitutes a very uncommon long period of high-energy waves for this stretch of coastline, combined with high wave angle with respect to shore-normal (between 15° and 20° W-NW). During this period the tidal range varied from spring (3.8 m) to neap (1.5 m) tide. During this 10-day period of high-energy waves ($Hs > 3$ m, $Tp > 12$ s), because of lower energy in comparison to the two previous storms, the outer bar developed crescentic patterns (down-state transition, D_o increased from 100 to 250 m, see Fig. 5b) and migrated some 200 m southward (Fig. 6). The outer-bar cross-shore migration was only minor. An up-state sequence of the inner-bar was observed, with decreasing alongshore non-uniformities (Figs. 4e and 5b).

Following this 4-storm sequence, waves remained low from April 1 to 9 with Hs lower than 2 m (Fig. 2). During this calm period, the outer bar was inactive, showing a moderate developed crescentic pattern (Fig. 3b), whereas the inner bar developed alongshore short-scale (~300 m) non-uniformities (Fig. 5a and b) (D_i increased to 80 m, Fig. 4f), with the development of shore-normal well-developed rip channels.

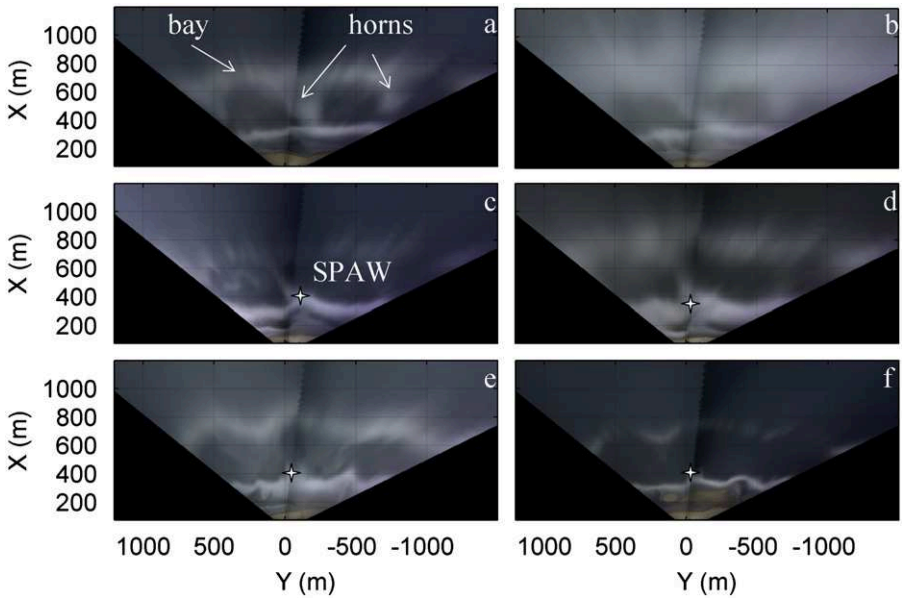

Fig. 4. Truc Vert Beach planview images on March (a) 8, (b) 12, (c) 14, (d) 22, April (e) 2 and (f) 7. The SPAW location is marked with a white star.

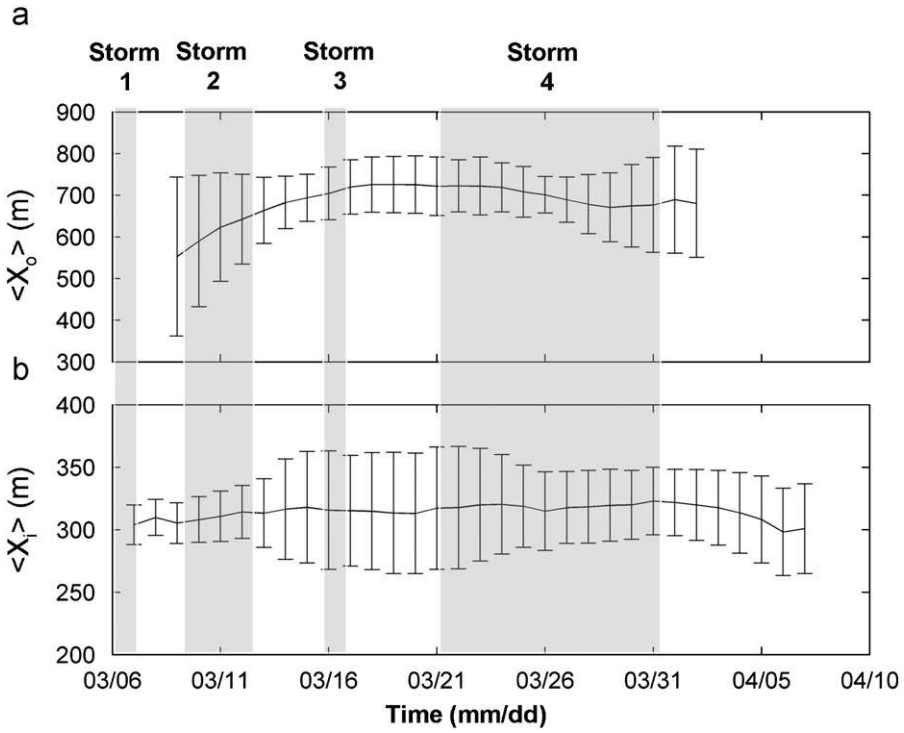

Fig. 5. Time series of outer (o) and inner bar (i) alongshore-averaged crest line cross-shore position ($\langle X \rangle$) with corresponding amplitudes (A) as errorbars for the (a) outer bar and (b) the inner bar.

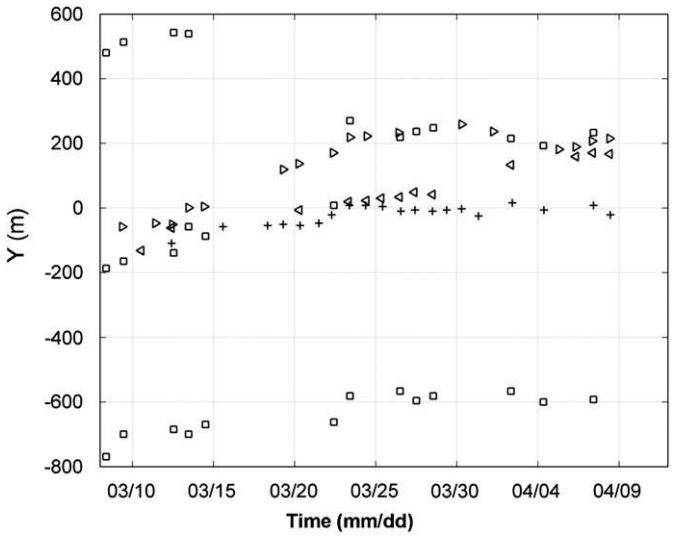

Fig. 6. Evolution over time of the alongshore position of the outer bar horns (squares), SPAW mean position (pluses) and rip feeder (left pointing triangles) and rip head (right pointing triangles).

3.2. SPAW dynamics

The destruction and evolution of the outer-bar horns initiated by the 10-year return storm on March 11–12 is further analyzed here. Prior to this storm, the outer-bar crescentic pattern was strongly developed with horns almost welded to the inner-bar (see Fig. 3). During the 10-year return storm, hourly video images showed that the outer bar experienced a clear reshaping into a more alongshore-uniform bar, comprising crescent horn shedding of bar-like feature from its shoreward facing side, whereas the seaward part migrated offshore. The SPAW transited the trough and merged with the inner bar (Fig. 4b and c). Despite its rapid creation (∼ hours) during the severe storm, the SPAW later evolved continuously and was clearly present until the end of the experiment, 3 weeks later (Fig. 4f).

During its existence, the SPAW did not migrate significantly in the alongshore direction, despite persistent high-energy oblique waves. The evolution of the SPAW contours shown in Fig. 7 indicates that, while the alongshore location remained constant, the area covered by the SPAW decreased continuously over time. The erosion of the feature was mainly localised at its seaward protruding part whereas the whole feature's geometry maintained alike, exhibiting a straight shore-normal oriented face. The SPAW's erosion is also indicated, in Fig. 8, by the evolution of its maximum length (L), which reduced from about 250 to 100 m (∼ −5 m/day).

To assess the longer-term (∼weeks) contribution of the SPAW to the intertidal morphology, the alongshore position of the SPAW was compared over time to the inner- and outer-bar feature positions (Fig. 6). From March 12 to 15, an outer-bar horn, the SPAW and an inner-bar rip channel were approximately aligned. During the long-duration storm from March 20 to 31, characterised by a 15° wave-incidence angle, both the outer-bar horns and the rip channels migrated southward whereas the SPAW and the inner-bar rip feeder channels did not migrate noteworthy. The following calm period induced a southward migration of the rip feeder channels, the rip channels orienting shore-normal. During this period, it is to be noted that inner-bar rip channels were facing the outer-bar horns (Fig. 4f). In contrast, the SPAW did not migrate. The fact that the inter-tidal bar migrated independently of the SPAW (located in the subtidal domain) during the following weeks after the SPAW generation clearly indicates that the SPAW did not control the weekly evolution of the inter-tidal morphology.

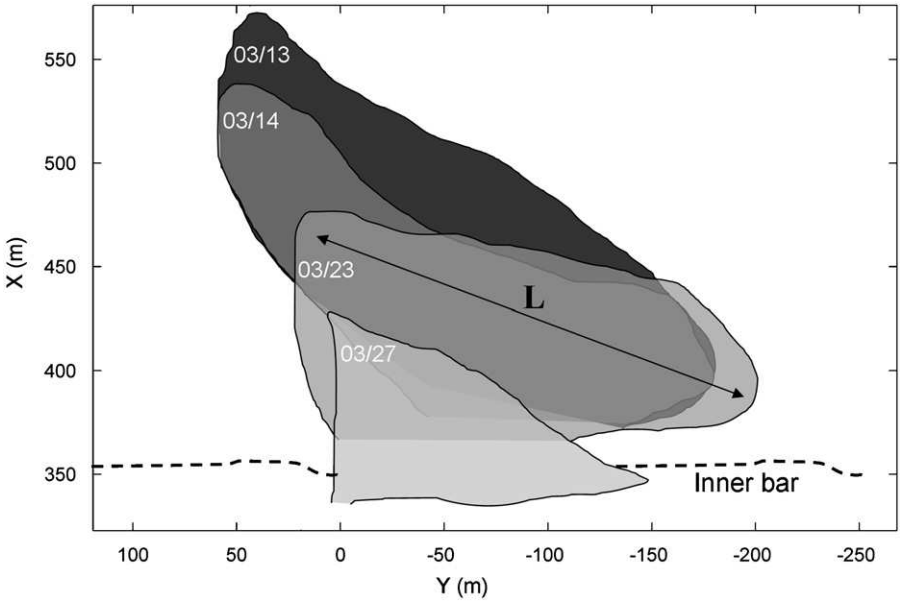

Fig. 7. Evolution over time of the SPAW geometry on March 13, 14, 23 and 27, ranging from dark to bright. The double-arrow represents the maximum length (L) of the SPAW.

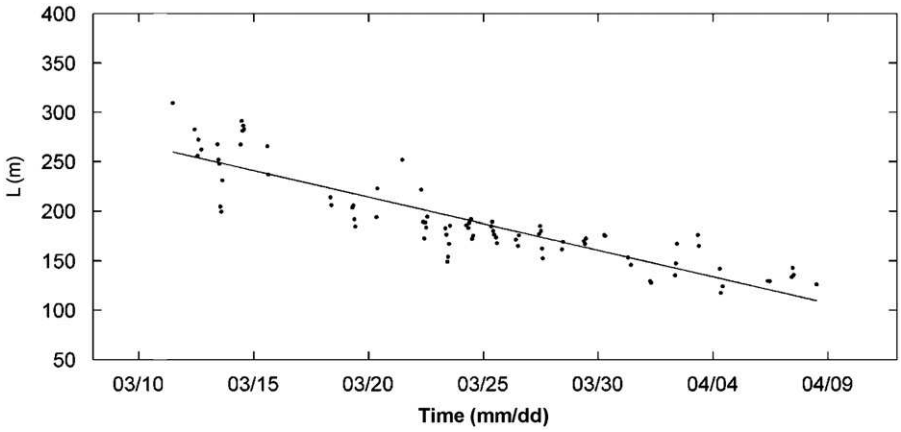

Fig. 8. Time evolution of the SPAW maximum length, L. The solid line represents the linear regression of L time series (slope = -5 m/day, R^2=0.58). SPAW was first observed on images from March 11.

3.3. *Morphological changes and link with offshore wave and tide forcing*

The offshore hydrodynamic HFI index (Eq. (1)) exhibited a large peak during the 10-year return storm (Fig. 9), due the combined effect of large *Hs* and large tidal range ($\sim$4 m). For the following storm (March 16), even though *Hs* was large ($Hs > 5$ m), the smaller tidal range ($\sim$2 m) substantially reduced HFI. During the long-duration storm (from March 21 to 31), moderate *Hs* reduced HFI even during large tidal range. On the whole study period, 52% of the MI variance was explained by *Hs* and 48% by d_{min} (Fig. 9).

In the meantime, the morphological change index MI (Eq. (4)) was maximum for the outer-bar (MI_o) during the 10-year return storm (Fig. 9) and minimum during the relatively calm period (from March 17 to 20). On the whole, 56% of the MI_o variability is explained by MI_{o2D} and 44% by MI_{o3D} (Eqs. (2) and (3), respectively). For the inner bar, the MI_i index time-evolution was clearly different, presenting maxima on March 14–15 and 24–25. In contrast to MI_o, the MI_i variability was rather more related to MI_{i3D} (71%) than to MI_{i2D} (29%).

Cross-correlation analysis was performed over the study period (35 points, 1 day^{-1}) between offshore wave- and tide-based indexes (*Hs*, HFI) and morphological indexes (MI_o and MI_i). Outer-bar changes (MI_o) are well correlated with *Hs* and HFI, as are MI_{o2D} and MI_{o3D} with a correlation maximum ($\sim$0.6, significant at the 95% level) at a 1–2 day time-lag. The fact that the correlation with HFI was not larger than with *Hs* indicates that tide-induced outer-bar changes were limited. In contrast, inner-bar changes (MI_i) were not significantly correlated with *Hs* (<0.2, not significant at the 95% level). Correlation was much larger with HFI, showing a maximum ($\sim$0.5, significant at the 95% level) at a 4–5 day time-lag. We found that correlation with HFI was larger for MI_{i3D} (0.7) than for MI_{i2D} (0.2). Thus, the inner-bar changes, and more particularly the 3D changes, were predominantly related to tidal range variations. This is discussed further in Section 4.3.

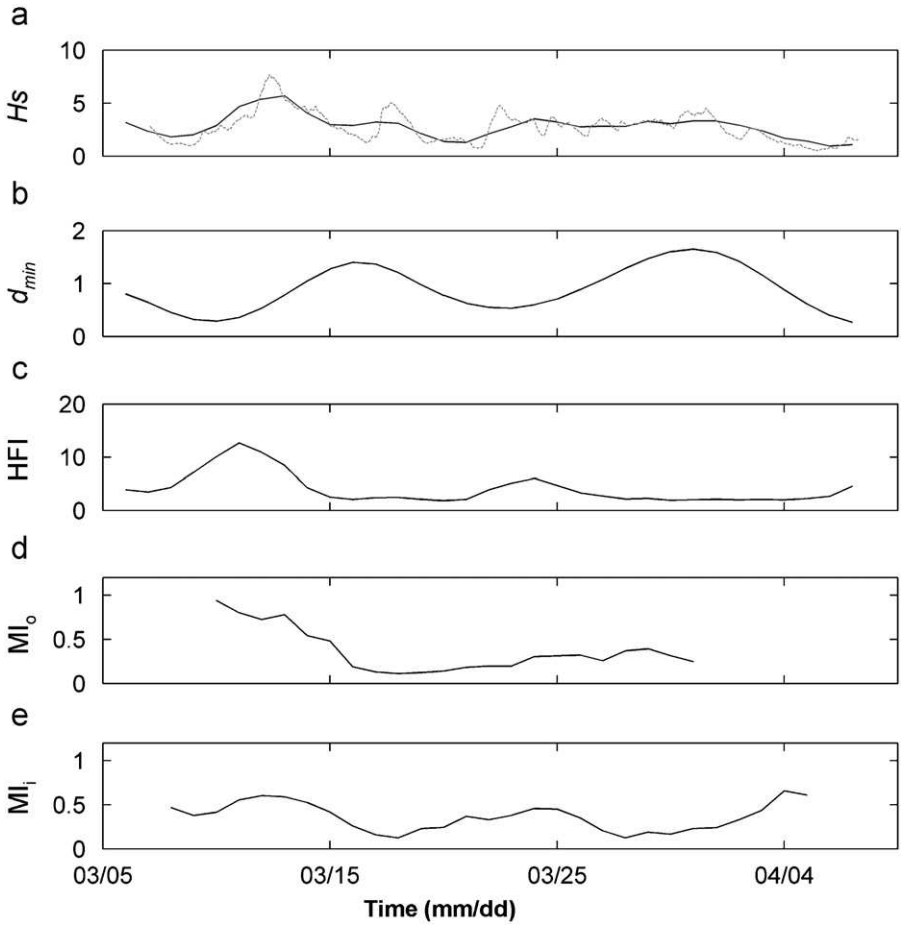

Fig. 9. Time evolution of (a) offshore significant wave height, H_s, (b) the lowest offshore water level experienced over a tidal cycle, d_{min}, (c) the HFI index, (d) the outer bar morphological variation indexes, MI_o, and (e) the inner bar morphological variation indexes, MI_i. The solid lines represent daily interpolated data and the dashed line in (a) represents the non daily-averaged offshore significant wave.

4. Discussion

4.1. Short term evolution of morphology

Our analysis of the ECORS08 TVB hourly video images dataset clearly shows that the double bar system response was highly variable with respect to which storm the beach was exposed to. This, together with the small correlation time-lag (~1–2 days) between the outer-bar changes (MI_o) and *Hs* contrasts with earlier studies at double-barred beaches that mentioned longer bar time response to storms. Observations reported in Ruessink et al. (2000) suggested a minor individual storm impact on the bars, the bars reacting to a sequence of storms rather to individual storm at a double-barred beach of Noordwijk (2–3 days smoothed observation by Van Enckevort and Ruessink, 2003a) and even longer time response spanning from 20 days to 1 year (Plant et al., 1999, 2006). The small response time observed at TVB may result from the exceptionally large waves experienced.

The distance between the inner bar and the outer-bar was close to 400 m at TVB which represents one of the largest observed values at double-barred beaches (~230 m at Noordwijk, Netherlands and ~100 m on the Gold Coast, Australia; Van Enckevort et al., 2004). Noteworthy, distances between bars in triple-barred systems can exceed 500 (Ruessink and Kroon, 1994; Ruggiero et al., 2005). The outer-bar seaward migration reached 30–50 m/day during high-energy wave conditions on March 11–12, a value close to the highest observed values at other sites (10–50 m/day, Van Enckevort and Ruessink, 2003a; Van Enckevort et al., 2004). These observations are not surprising given that TVB was exposed to a 10-year return storm. The rapid and large offshore migration, assumed to be the result of a breakpoint adjustment mechanism, was increased by the large distance between bar position and offshore located breakpoint at the beginning of the storm.

The observed large offshore alongshore-averaged bar migration resulted from the straightening of the pre-existing crescentic pattern rather than from the offshore migration of the entire bar. In other words, the bays did not significantly migrate in the cross-shore direction but the outer-bar amplitude decreased, the horns being more dynamic than the bays (Fig. 10). We developed a simple model to describe the alongshore-averaged cross-shore bar migration by separating the contributions of the two processes: the bar cross-shore migration and the bar three-dimensional development. The first contribution is defined in the model as the position of the bays, $\langle X_{bays} \rangle$, and the second contribution is kD, a linear dependence on the distance between bays and horns. The alongshore-averaged bar position can be approximated as

$$\langle X \rangle = \langle X_{bays} \rangle - kD \quad (5)$$

Fitting the data from the outer bar to Eq. (5) results in $k=0.3$ with a good agreement between the reconstructed and actually observed alongshore-averaged outer-bar position (Fig. 11): Eq. (5) captures 92% of the total variance in $\langle X \rangle$. This indicates that our

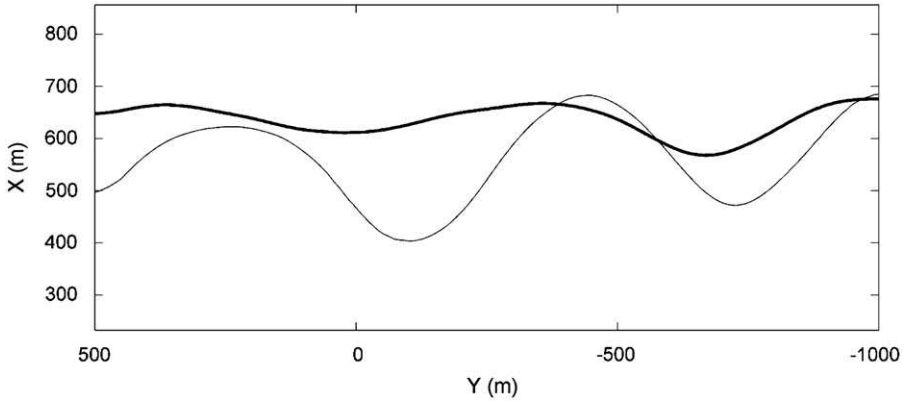

Fig. 10. Video-digitized position of the TVB outer bar crest on March 8 (thin line) and March 13 (thick line), respectively, before and after the 10-year return storm.

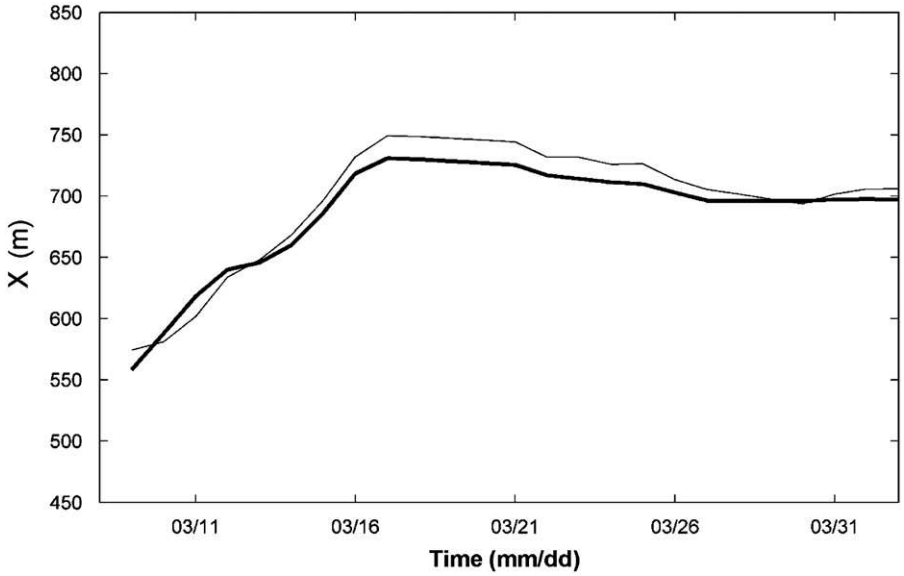

Fig. 11. Time series of outer-bar alongshore-averaged position ($\langle X \rangle$) (thin line) and reconstructed position from Eq. (5), with k=0.3 (thick line).

simple model is appropriate for the description of the bar position, the coefficient k being a good descriptor for the separation of 2D and 3D contributions to the bar migration. Most certainly, this coefficient is site-dependent. For the study period, $\langle X_{bays} \rangle$ and kD explained 55% and 37% of the observed $\langle X \rangle$ variance, respectively. Thus, the different response of horns and bays contributed considerably to the observed overall cross-shore migration of the outer bar. This observed non-linear evolution suggests that bar behaviour is even more complex than previously envisaged, in particular when considering the bar response to storms, which is different from a whole migration or a symmetric (bar horns) amplitude reduction. Our observation that offshore sandbar migration during a storm might result from a differential response of bays and horns contrasts with the commonly held view from field (e.g., Gallagher et al., 1998) and model studies (e.g., Ruessink et al., 2007b) that offshore migration is purely 2D.

With respect to the inner bar, we observed large inner-bar 3D changes (71% of total changes) associated with small alongshore-averaged cross-shore migration. This result can be related to the findings of Ruessink et al. (2000) who showed that, for the inner bar at Egmond aan Zee (Netherlands), 85% of the variance in the inner-bar crest short-term changes corresponded to alongshore non-uniformity variations or alongshore migration whereas only 10% were associated to alongshore-averaged cross-shore migration.

4.2. Morphological interactions

4.2.1. SPAW generation

The mechanism leading to the formation of the SPAW is not understood. Existing SPAW observations (Wijnberg and Holman, 2007; Shand, 2007) report the presence of well developed 3D bar geometries prior to the SPAW formation. In a study on transverse-bars dynamic, Konicki and Holman (2000) found that, under some conditions, well developed 3D bar horns may detach and either dissipate within the trough or migrate landward. Wave incidence angle and resulting alongshore current are believed to play a key role in the SPAW formation and trough transiting. The conditions at TVB and Duck during SPAW formation are intense wave forcing combined with well-developed outer-bar crescents. This is confirmed tentatively by the numerical modelling study of Castelle (2004). In a model run with Hs=4 m and a well-developed crescentic outer-bar (vertical amplitude of the horn/bay sequence of about 3.5 m) at t=7 days, he obtained a local shoreward propagation of sediment resulting from horn degeneration, similar to the observed SPAW events. This behaviour was not

observed for lower (yet energetic) waves (for instance, $Hs=3$ m), neither for weakly- to reasonably-developed crescentic patterns (for the $Hs=4$ m run, for instance at $t=5$ days when the vertical amplitude of the horn/bay sequence amounted 2 m). Castelle (2004) numerical study was not set up specifically to study SPAW behaviour and the SPAW generation mechanism, therefore, remains unclear.

At TVB, the SPAW required only 1 day to transit the trough and merge to the inner-bar whereas a much longer time was reported for Duck (17 days on average, Wijnberg and Holman, 2007). This rapid propagation is believed to be related to exceptionally large waves at TVB, but also to the pre-existing well-developed crescentic outer-bar geometry comprising horns that were, prior to the severe storm, already very close to the inner bar ($\sim$50 m).

4.3. SPAW control on the inner bar

The SPAW represented a large input of sediment for the inner bar and the whole intertidal area. This suggestion has been verified with the computation of the surveyed intertidal beach volume changes facing the SPAW. Local total accretion was up to +30 000 m^3 at a rate that reached 10 000 m^3/day rapidly after the peak of the storm (on March 12–13; Capo et al., 2009) whereas the remainder of the intertidal beach (outside of the SPAW influence) eroded (up to -27 m^3/m; Capo et al., 2009). In line with observations reported by Shand (2007), this clearly suggests that a SPAW causes a major input of sand into the intertidal domain, preventing a stretch of beach from eroding even during intense wave forcing.

During the storm (March 16–17) following the SPAW generation, the alongshore non-uniformity in the inner bar evolved from being large-scale and low-amplitude into short-scale and high-amplitude. The formation of intertidal non-uniformities has previously been related to a nearshore topography readjustment of excess sediment (Komar, 1998). This point suggests that the massive input of sand to the inter-tidal area during the large storm (March 11) re-arranged during the following storm (March 16–17). Moreover, the fact that the outer bar was almost alongshore uniform during the second storm acts in favour of a self-organization origin of the development of the inner-bar non-uniformities rather than a morphological coupling (template) origin.

The SPAW was still present 3 weeks later at the same location (Fig. 7). However, the longer-term ($\sim$weeks) impact of the SPAW on the inner-bar morphology is less understood. More generic conclusions about the SPAW contribution on the double bar dynamics are limited by the short alongshore distance of the video monitored inner-bar area ($\sim$1000 m, Fig. 3). Yet, the fact that intertidal features migrated southward and that the subtidal SPAW feature remained at the same position suggests that the inter-tidal bar rapidly evolved independently of the SPAW. In addition, our results indicate that during the storm from March 20 to 30, the tracked inner-bar rip channel migrated southward, facing an outer-bar horn (Fig. 6). This is consistent with observations by Van Enckevort and Wijnberg (1999) and numerical modelling (Castelle et al., in press-a) who indicated that inner- and outer-bar out-of-phase coupling can occur in the presence of well-developed outer-bar crescentic patterns and moderate energy waves. Our results suggest that the short-term contribution of the SPAW event to the inner-bar was a large input of sediment that re-arranged within days into short-scale features. The longer-term ($\sim$weeks) contribution was not substantial although the SPAW remained present after 3 weeks. The evolution of inter-tidal morphology during the storm from March 20 to 30 is assumed to be rather controlled by the developing outer-bar crescents, in a similar manner as documented by Ruessink et al. (2007a).

4.4. Tidal influence

The outer-bar changes were predominantly linked to *Hs*, and although the correlation was slightly higher considering a combination of *Hs* and d_{min} (HFI) there was no clear evidence of any tide contribution to outer-bar changes. In our data, we believe that the effect of d_{min} may have been negligible because waves were always breaking when the bar was morphologically most active. In contrast, the inner-bar changes were more strongly related to HFI than to *Hs*, similar to findings in the intertidal-bar dynamics study of Kroon and Masselink, (2002) where intertidal-bar dynamics was found to be controlled by both *Hs* and the tidal range. We hypothesise that, in our observations, the observed stronger influence of tide on the inner-bar dynamics was caused by the combined effects of large tidal range variations, large waves and the presence of the subtidal bar. Firstly, as reported in Masselink et al. (2008) for TVB, the large subtidal bar protects the intertidal beach from exposure to extreme wave conditions, thus, inshore significant wave heights are generally less than 2.5 m. During almost the entire campaign, waves broke on the outer bar. When the tidal range was small, the inner bar was persistently in the surf zone. During mid to spring tidal conditions, the inner bar experienced swash conditions at low tide. Thus, in contrast to the outer bar, the tidal range affected the residence times of breaking waves and swash processes, and this likely explains the larger effect of HFI on inner than on outer-bar behaviour. For these reasons, tidal range variations were crucial to the evolution of the inner bar.

We found an even higher correlation coefficient value for MI_i and d_{min} (0.6) than with *HFI* or *Hs*. Noteworthy, the peak of correlation between MI_i and d_{min} was present for a 5-day lag. This time-lag is close to a quarter of the neap-spring tide cycle period (28 days) indicating that inner-bar changes maxima occurred when the tide range changed from spring tide to neap tide ($\max(\partial d_{min}/\partial t)$). The observed peaks in MI_i may thus be attributed to transitions from a persisting high-tidal range regime to a small-tidal range regime. This peak of MI_i did not appear from neap to spring tide (near March 20), presumably because the waves were too small ($Hs<1$ m) to induce beach change.

5. Conclusions

We analyzed a 5-week dataset of hourly, 10-min time-exposure video images of the double-barred meso–macro tidal Truc Vert Beach during intense wave forcing, comprising a 10-year return storm. The short-term (days) response of the outer, subtidal bar to the storms was significant and rapid (1–2 days) for both the dominant (56% of total changes) 2D component with an observed 30–50 m/day maximum seaward migration rate, and for the 3D component (44%), comprising a reshaping of the crescentic patterns into a shore-parallel linear bar. We found that the 3D behaviour influenced the 2D behaviour (37%). In particular, the rapid seaward migration of the alongshore-averaged crest position was partially due to the seaward migration of the horns (reshaping crescents into a shore-parallel linear bar), while the bays did not migrate substantially. This contrasts with the common perception that the bar, as a whole, migrate seaward during storm events. Inner-bar dynamics was dominated by 3D changes (71% of total changes) comprising the local merging of a SPAW (a former outer-bar horn) and the development of alongshore non-uniformities. The inner-bar 2D component (29% of total changes) was associated with cross-shore migration

rates of less than 5 m/day. Whereas outer-bar changes were primarily governed by *Hs* variability, the tidal range appeared to be the steering parameter for inner-bar changes.

The straightening of the outer bar during the most intense storm strongly affected the subsequent evolution of the inner bar. The SPAW represented a large input of sediment for the inter-tidal area. Three weeks later, although the subtidal SPAW remaining feature was still present and attached to the intertidal bar, inter-tidal bar pattern showed no evidence of forcing by the SPAW template any more. We believe that the generation of the SPAW was stimulated by the well-developed outer-bar crescentic pattern before the storm.

In summary, our results indicate that inner-bar behaviour depends on the morphological setting prior to the main storm (the presence of a subtidal bar and its well-developed crescentic shape) and the tide range rather than on storm characteristics only. Inner and outer bars should, therefore, not be studied in isolation.

Acknowledgments

The ECORS experiment and TVB video system were supported by the French "Service Hydrographique et Oceanographique de la Marine" (SHOM). RA's Ph.D. work is funded by the French "Délégation Générale de l'Armement" (DGA). BC and PB acknowledge financial support from the Project MODLIT (RELIEFS/INSU). BGR was supported by the Netherlands Organisation for Scientific Research NWO under project 864.04.007.

References

Aagaard, T., Nielsen, J., Greenwood, B., 1998. Suspended sediment transport and nearshore bar formation on a shallow intermediate-state beach. Mar. Geol. 148, 203–225.

Aarninkhof, S.G.J., Hinton, C.L., Wijnberg, K.M., 1998. On the predictability of breaker bar behaviour. In: Proceedings of the 26th International Conference on Coastal Engineering, Copenhagen, Denmark, ASCE, pp. 2409–2422.

Butel, R., Dupuis, H., Bonneton, P., 2002. Spatial variability of wave conditions on the French Atlantic coast using in-situ data. J. Coastal Res. SI 36, 96–108.

Capo, S., Parisot, J.-P., Bujan, S., Senechal, N., 2009. Short time morphodynamics response of the Truc Vert Beach to storm conditions. J. Coastal Res. SI 36, 1741–1745.

Castelle, B., 2004. Modélisation de l'hydrodynamique sédimentaire au-dessus des barres sableuses soumises à l'action de la houle: application à la côte aquitaine. Ph.D. thesis, Université Bordeaux I, pp. 340 (in French).

Castelle, B., Bonneton, P., Dupuis, H., Sénéchal, N., 2007. Double bar beach dynamics on the high-energy meso–macrotidal French Aquitanian Coast: a review. Mar. Geol. 245, 141–159.

Castelle, B., Ruessink, B.G., Bonneton, P., Marieu, V., Bruneau, N., Price, T.D. (in press-a). Coupling mechanisms in double sandbar systems, Part 1: physical explanation and coupling patterns. Earth Surf. Processes Landforms, doi:10.1002/esp.1929.

Castelle, B., Ruessink, B.G., Bonneton, P., Marieu, V., Bruneau, N., Price, T.D. (in press-b). Coupling mechanisms in double sandbar systems, Part 2: impact on alongshore variability of inner-bar rip channels. Earth Surf. Processes Landforms, doi:10.1002/esp.1949.

Coco, G., Murray, A.B., 2007. Patterns in the sand: from forcing templates to self-organization. Geomorphology 91, 271–290.

De Melo Apoluceno, D., Howa, H., Dupuis, H., Oggian, G., 2002. Morphodynamics of ridge and runnel systems during summer. J. Coastal Res. SI 36, 222–230.

De Melo Apoluceno, D., 2003. Morpho-hydrodynamique des plages à barres en domaine méso à macrotidal: exemple de la plage du Truc Vert-Gironde. Ph.D. Thesis, Université Bordeaux I (in French).

Desmazes, F., Michel, D., Howa, H., Pedreros, R., 2002. Etude morphodynamique du domaine pré-littoral nord-aquitain, site atelier du Truc Vert. In: Proc. 7ème Journées Nationales GCGC, Anglet, pp. 155–162 (in French).

Froidefond, J.-M., Gallissaires, J.-M., Prud'homme, R., 1990. Spatial variation in sinusoidal on a crescentic nearshore bar: application to the Cap Ferret Coast. J. Coastal Res. 6, 927–942.

Gallagher, E.L., Elgar, S., Guza, R.T., 1998. Observations of sand bar evolution on a natural beach. J. Geophys. Res. 103, 3203–3210.

Holland, K.T., Holman, R.A., Lippmann, T.C., Stanley, J., Plant, N., 1997. Practical use of video imagery in nearshore oceanographic field studies. IEEE J. Oceanic Eng. Oceanic Eng. 22, 81–92.

King, C.A.M., Williams, W.W., 1949. The formation and movement of sand bars by wave action. Geogr. J. 112, 70–85.

Komar, P.D., 1998. Beach Processes and Sedimentation. Prentice-Hall, Englewood Cliffs, New Jersey.

Konicki, K.M., Holman, R.A., 2000. The statistics and kinematics of transverse sand bars on an open coast. Mar. Geol. 169, 69–101.

Kroon, A., Masselink, G., 2002. Morphodynamics of intertidal bar morphology on a macrotidal beach under low-energy wave conditions, North Lincolnshire, England. Mar. Geol. 190, 573–591.

Lafon, V., Dupuis, H., Howa, H., Froidefond, J.-M., 2002. Determining ridge and runnel longshore migration rate using spot imagery. Oceanol. Acta 25, 149–158.

Lafon, V., De Melo Apoluceno, D., Dupuis, H., Michel, D., Howa, H., Froidefond, J.-M., 2004. Morphodynamics of nearshore rhythmic sandbars in a mixed-energy environment (Sw France).i. mapping beach changes using visible satellite imagery. Estuarine Coastal Shelf Sci. 61, 289–299.

Lippmann, T.C., Holman, R.A., 1989. Quantification of sandbar morphology: a video technique based on wave dissipation. J. Geophys. Res. 94, 995–1011.

Masselink, G., Short, A.D., 1993. The effect of tide range on beach morphodynamics and morphology: a conceptual beach model. J. Coastal Res. 9, 785–800.

Masselink, G., Turner, I.L., 1999. The effect of tides on beach morphodynamics. In: Short, A.D. (Eds.), Handbook of Beach and Shoreface Morphodynamics Wiley.

Masselink, G., 2004. Formation and evolution of multiple bars on macrotidal beaches: application of a morphodynamic model. Coastal Eng. 51, 713–730.

Masselink, G., Kroon, A., Davidson-Arnott, R.G.D., 2006. Intertidal bar morphodynamics in wave-dominated coastal settings: a review. Geomorphology 73, 3349.

Masselink, G., Auger, N., Russel, P., O'Hare, T., 2007. Short-term morphological change and sediment dynamics in the intertidal zone of a macro-tidal beach. Sedimentology 54, 39–53.

Masselink, G., Austin, M., Tinker, J., O'Hare, T., Russell, P., 2008. Cross-shore sediment transport and morphological response on a macro-tidal beach with intertidal bar morphology, Truc Vert, France. Mar. Geol. 251, 141–155.

Owens, E.H., Frobel, D.H., 1977. Ridge and runnel systems in the Magdalen Islands. Que. J. Sediment Petrol. 47, 191–198.

Pape, L., Ruessink, B.G., 2008. Multivariate analysis of nonlinearity in sandbar behavior. Nonlinear Processes Geophys. 15, 145–158.

Parisot, J.-P., Capo, S., Bujan, S., Sénéchal, N., Moreau, J., Réjas, A., Hanquiez, V., Almar, R., Marieu, V., Castelle, B., Gaunet, J., Gluard, L., George, I., Nahon, A., Dehouck, A., Certain, R., Gervais, M., Barthe, P., Ardhuin, F., Le Gall, F., Bernardi, P.J., Le Roy, R., Pedreros, R., Delattre, M., Mac Mahan, J., 2009. Sedimentary processes and morphodynamics of sandy beaches on short time response. J. Coastal Res. SI 56, 1786–1790.

Pedreros, R., Howa, H.L., Michel, D., 1996. Application of grain size trend analysis for the determination of sediment transport pathways in intertidal areas. Mar. Geol. 135, 35–49.

Plant, N.G., Holman, R.A., Freilich, M.H., Birkemeier, W.A., 1999. A simple model for interannual sandbar behavior. J. Geophys. Res. 104 (15), 755–776.

Plant, N.G., Freilich, M.H., Holman, R.A., 2001. Role of morphologic feedback in surf zone sandbar response. J. Geophys. Res. 106 (C1), 973–989.

Plant, N.G., Holland, K.T., Holman, R.A., 2006. A dynamical attractor governs beach response to storms. Geophys. Res. Lett. 33, L17607.

Price, T.D., Ruessink, B.G., 2008. Morphodynamic zone variability on a microtidal barred beach. Mar. Geol. 251, 98–109.

Ruessink, B.G., Kroon, A., 1994. The behaviour of a multiple bar system in the nearshore zone of Terschelling: 1965–1993. Mar. Geol. 121, 187–197.

Ruessink, B.G., Terwindt, J.H.J., 2000. The behaviour of nearshore bars on the time scale of years: a conceptual model. Mar. Geol. 163, 289–302.

Ruessink, B.G., Van Enckevort, I.M.J., Kingston, K.S., Davidson, M.A., 2000. Analysis of observed two- and three-dimensional nearshore bar behaviour. Mar. Geol. 169, 161–183.

Ruessink, B.G., Wijnberg, K.M., Holman, R.A., Kuriyama, Y., Van Enckevort, I.M.J., 2003. Intersite comparison of interannual nearshore bar behavior. J. Geophys. Res. 108, 3249.

Ruessink, B.G., Coco, G., Ranasinghe, R., Turner, I.L., 2007a. Coupled and noncoupled behavior of three-dimensional morphological patterns in a double sandbar system. J. Geophys. Res. 112, C07002.

Ruessink, B.G., Kuriyama, Y., Reniers, A.J.H.M., Roelvink, J.A., Walstra, D.J.R., 2007b. Modeling cross-shore sandbar behavior on the time scale of weeks. J. Geophys. Res. 112, F03010, doi:10.1029/2006JF000730.

Ruggiero, P., Kaminsky, G.M., Gelfenbaum, G., Voigt, B., 2005. Seasonal to interannual morphodynamics along a high-energy dissipative littoral cell. J. Coastal Res. 21 (3), 553–578.

Sallenger, A.H., Holman, R.A., Birkemeier, W.A., 1985. Storm-induced response of a nearshore-bar system. Mar. Geol. 64, 237–257.

Sénéchal, N., Ardhuin, F., and others, 2008. ECORS-TRUC VERT, 2008. Qualification des modèles de houle et de morphodynamique. In: Proc 10èmes Journées Nationales GCGC, pp. 635–654 (in French).

Sénéchal, N., Gouriou, T., Castelle, B., Parisot, J.P., Capo, S., Bujan, S., Howa, H., 2009. Morphodynamic response of a meso- to macro-tidal intermediate beach based on a long-term data-set. Geomorphology 107, 263–274.

Shand, R.D., 2007. Bar splitting: system attributes and sediment budget implications for a net offshore migrating bar system. J. Coastal Res. SI 50.

Short, A.D., 1991. Macro–Meso tidal beach morphodynamics—an overview. J. Coastal Res. 72, 417–436.

Short, A.D., Aagaard, T., 1993. Single and multi-bar beach change models. J. Coastal Res. IS 15, 141–157.
Van Enckevort, I.M.J., Ruessink, B.G., 2001. Effect of hydrodynamics and bathymetry on video estimates of nearshore sandbar position. J. Geophys. Res. 106, 16969–16980.
Van Enckevort, I.M.J., Ruessink, B.G., 2003a. Video observations of nearshore bar behaviour. Part 1: alongshore uniform variability. Cont. Shelf Res. 23, 501–512.
Van Enckevort, I.M.J., Ruessink, B.G., 2003b. Video observations of nearshore bar behaviour. Part 2: alongshore non-uniform variability. Cont. Shelf Res. 23, 513–532.
Van Enckevort, I.M.J., Ruessink, B.G., Coco, G., Suzuki, K., Turner, I.L., Plant, N.G., Holman, R.A., 2004. Observations of nearshore crescentic sandbars. J. Geophys. Res. 109, C06028.
Van Enckevort, I.M.J., Wijnberg, K.M., 1999. Intra-annual changes in bar plan shape in a triple bar system. In: Proceedings of the Coastal Sediments '99, ASCE, pp. 2548–2558.
Wijnberg, K.M., Holman, R.A., 2007. Video-observations of shoreward propagating accretionary waves. In: Proceedings of the RCEM 2007, Enschede, The Netherlands, pp. 737–743.
Wright, L.D., Short, A.D., 1984. Morphodynamic variability of surf zones and beaches: a synthesis. Mar. Geol. 56, 93–118.